JOURNAL OF COMPUTATIONAL PHYSICS 16, 49–65 (1974)

Numerical Simulation of a Radially Inhomogeneous Cylindrical Plasma

D. W. HEWETT*

Department of Physics and Astronomy, University of Kansas, Lawrence, Kansas 66044

Received October 11, 1973; revised February 25, 1974

The numerical time integration of an initial value problem based upon the nonlinear Vlasov equation as applied to an axisymmetric, inhomogeneous plasma column has been developed. All six components of the electric and magnetic fields are advanced self-consistently in time. An assumption has been made which neglects purely electromagnetic modes. Each field contains a contribution from plasma source terms calculated by a Green's function technique as well as a boundary value contribution which may be time dependent. The Vlasov equation has been reduced to a convenient numerical form by an extension of the standard Fourier–Hermite expansion. Radial dependence is discretized. Results are presented on the streaming instability of the electrostatic column.

The need for a general technique to simulate cylindrical, radially inhomogeneous plasma columns has arisen from the present research in controlled thermonuclear fusion. Multidimensional problems have proven too complex for general analytic analysis and have been simulated numerically by a variety of techniques, most of which are based upon calculation of individual particle trajectories [1]. Maintaining sufficiently small statistical noise levels in these simulations requires large numbers of particles (severely taxing even the best computational facilities). We describe herein an economic alternative for simulating some aspects of the nonlinear behavior of a plasma column in a 5-D phase space (ρ, z, v_ρ, v_ϕ, v_z) by transform methods. Provisions are made to advance both the plasma dynamics in 2-D as well as all six components of the electric and magnetic field (neglecting purely radiative mdes) in time.

The applications of such a computer code to present CTR experiments appear to be numerous. The obvious difficulties associated with multidimensional simulation are the expected requirements of large computer memory and long running times. Such requirements have not proven to be excessive by present standards since the electrostatic column results discussed here and elsewhere [2, 3] have been obtained with not more than 20,000 single precision words to represent

* Permanent address: CTR-6, LASL, Los Alamos, NM.

the plasma and field quantities and less than 50,000 single precision words for the entire running code. Run times have been approximately 40 sec per axial plasma period (ω_p^{-1}) on a Honeywell 635.

I. Model and Basic Equations

The model which serves as a basis for the simulation is shown in Fig. 1. The diffuse boundary column is represented on a grid extending to $\rho = a$; and external fields may be applied by fixing the appropriate boundary conditions on the surface $\rho = b$. It is assumed that no significant plasma source currents or charges exist in the region between $\rho = a$ and $\rho = b$. As already discussed, the column is independent of azimuth; and anticipating the Fourier expansion of the axial z dependence, only one periodicity length L of the axial coordinate is displayed. The existing computer code functions with the assumption of mirror symmetry on each end of L (though there is no fundamental difficulty in relaxing this requirement).

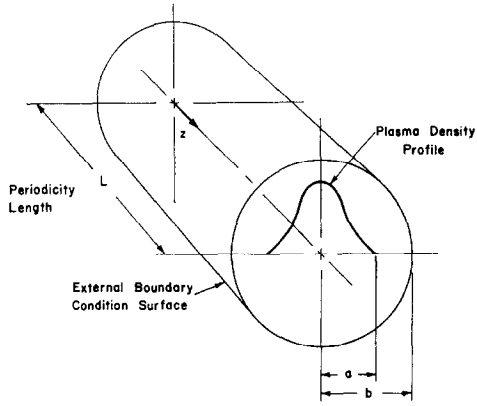

FIG. 1. The cylindrical model.

The simulation is based upon the dimensionless cylindrical Vlasov equation for electrons:

$$\frac{\partial f}{\partial t} + v_\rho \frac{\partial f}{\partial \rho} + v_z \frac{\partial f}{\partial z} + \frac{v_\phi^2}{\rho} \frac{\partial f}{\partial v_\rho} - \frac{v_\rho v_\phi}{\rho} \frac{\partial f}{\partial v_\phi} - (v_\phi B_z - v_z B_\phi + E_\rho) \frac{\partial f}{\partial v_\rho}$$
$$- (v_z B_\rho - v_\rho B_z + E_\phi) \frac{\partial f}{\partial v_\phi} - (v_\rho B_\phi - v_\phi B_\rho + E_z) \frac{\partial f}{\partial v_z} = \frac{\partial f}{\partial t}\bigg|_c . \qquad (1)$$

The equation has been scaled in terms of the electron plasma frequency $\omega_p^2 = (4\pi q^2 N_{\text{axial}}/m)$, the electron thermal velocity ($v_{\text{th}}^2 = 3kT/m$), and the plasma length ($\lambda_D = v_{\text{th}}/\omega_p$) as follows:

$$\mathbf{B} \to (m\omega_p/q)\, c\mathbf{B}, \tag{2}$$

$$\mathbf{E} \to (m\omega_p/q)\, v_{\text{th}}\mathbf{E}, \tag{3}$$

$$f \to f(v_{\text{th}}^3 \lambda_D^3/N_a), \tag{4}$$

$$\mathbf{x} \to \lambda_D \mathbf{x}, \tag{5}$$

$$\mathbf{v} \to v_{\text{th}}\mathbf{v}, \tag{6}$$

$$t \to (t/\omega_p). \tag{7}$$

The fields must be solutions of Maxwell's equations, here written as the vector inhomogeneous wave equations

$$\left(\nabla^2 - \frac{1}{c^2}\frac{\partial^2}{\partial t^2}\right)\begin{pmatrix}\mathbf{E}\\ \mathbf{B}\end{pmatrix} = \begin{pmatrix}\nabla\tilde{\rho} + \dfrac{1}{c^2}\dfrac{\partial \mathbf{j}}{\partial t}\\ -\dfrac{1}{c^2}\nabla \times \mathbf{j}\end{pmatrix} \tag{8}$$

with the charge and current densities given by

$$\tilde{\rho} = \int d\mathbf{v}\,(f^i - f), \tag{9}$$

$$\mathbf{j} = -\int d\mathbf{v}\,\mathbf{v}f. \tag{10}$$

The ions $f^i(\rho, z)$ constitute an immobile positive background.

Reduction of this set of equations to a numerical algorithm begins with the Fourier expansion of the axial dependence of all quantities; that is,

$$\begin{Bmatrix} f(\rho, z, v_\rho, v_\phi, v_z, t)\\ \mathbf{E}(\rho, z, t)\\ \mathbf{B}(\rho, z, t)\\ \tilde{\rho}(\rho, z, t)\\ \mathbf{j}(\rho, z, t)\end{Bmatrix} = \sum_n \exp(inkz) \begin{Bmatrix} f_n(\rho, v_\rho, v_\phi, v_z, t)\\ \mathbf{E}_n(\rho, t)\\ \mathbf{B}_n(\rho, t)\\ \tilde{\rho}_n(\rho, t)\\ \mathbf{j}_n(\rho, t)\end{Bmatrix}. \tag{11}$$

The Kinetic Equation

Each Fourier component of the distribution function $f_n(\rho, v_\rho, v_\phi, v_z, t)$ is now expanded in a triple Hermite series as

$$f_n(\rho, v_\rho, v_\phi, v_z, t) = \sum_{s,q,r=0}^{\infty} \exp[-(v_\rho^2 + v_\phi^2 + v_z^2/\sigma)/2]\, h_q(v_\rho)\, h_r(v_\phi)\, h_s(v_z)\, Z_{s,q,r,n,n}(t). \tag{12}$$

The Hermite polynomials are orthonormal for the weight function $\exp(-v^2/2\sigma)$. σ is unity for the v_ρ and v_ϕ series. The radial dependence of f_n is discretized on the radial grid ρ_η.

Hereafter, the Z coefficients will be assumed to have the subscript set (s, q, r, η, n). Explicit subscripts will be displayed only for those indices differing from this set. Substituting these expansions into (1), we have

$$\begin{aligned}
\frac{d}{dt} Z(t) = & -q^{1/2} \frac{\Delta}{\Delta\rho} Z_{q-1}\Big|_{\rho_\eta} - (q+1)^{1/2} \frac{\Delta}{\Delta\rho} Z_{q+1}\Big|_{\rho_\eta} \\
& + \frac{q^{1/2}}{\rho_\eta} [(r+2)^{1/2}(r+1)^{1/2} Z_{q-1,r+2} + rZ_{q-1}] \\
& - \frac{(q+1)^{1/2}}{\rho_\eta} [(r+1) Z_{q+1} + (r-1)^{1/2} r^{1/2} Z_{q+1,r-2}] \\
& - ink\,\sigma \left[\left(\frac{s}{\sigma}\right)^{1/2} Z_{s-1} + \frac{(s+1)^{1/2}}{\sigma} Z_{s+1}\right] \\
& - \sum_{n'} \Big\{ q^{1/2} \Big[(r+1)^{1/2} B^z_{\eta,n-n'} Z_{q-1,r+1,n'} + E^\rho_{\eta,n-n'} Z_{q-1,n'} \\
& - B^\phi_{\eta,n-n'} \left(\left(\frac{s}{\sigma}\right)^{1/2} (\sigma - 1) Z_{s-1,q-1,n'} + \sigma \left(\frac{s+1}{\sigma}\right)^{1/2} Z_{s+1,q-1,n'}\right)\Big] \\
& + r^{1/2} \Big[-(q+1)^{1/2} B^z_{\eta,n-n'} Z_{q+1,r-1,n'} + E^\phi_{\eta,n-n'} Z_{r-1,n'} \\
& + B^\rho_{\eta,n-n'} \left(\left(\frac{s}{\sigma}\right)^{1/2} (\sigma - 1) Z_{s-1,r-1,n'} + \sigma \left(\frac{s+1}{\sigma}\right)^{1/2} Z_{s+1,r-1,n'}\right)\Big] \\
& + \left(\frac{s}{\sigma}\right)^{1/2} [(q+1)^{1/2} B^\phi_{\eta,n-n'} Z_{s-1,q+1,n'} + E^z_{\eta,n-n'} Z_{s-1,n'} \\
& - (r+1)^{1/2} B^\rho_{\eta,n-n'} Z_{s-1,r+1,n'}]\Big\} + \frac{\delta Z_{n'}}{\delta t}\Big|_c . \qquad (13)
\end{aligned}$$

The derivative with respect to radius is now accomplished with centered finite differencing represented by the operator Δ. More discussion of the grid and grid-determined techniques will be presented in later sections.

It is obvious that even for a few terms in each expansion, the five-subscripted, complex Z array will require large amounts of computer memory. The storage is halved by using a perfect reflection condition, formally $f(\rho, z, v_\rho, v_\phi, v_z, t) =$

$f(\rho, -z, v_\rho, v_\phi, -v_z, t)$. Using this, coupled with the reality condition, we find $Z_{sqrnn}(t)$ is purely real (imaginary) when s is even (odd). Reflection symmetry also produces the additional advantage that only the real parts of $E_n{}^\rho$, $E_n{}^\phi$ and $B_n{}^z$ and the imaginary parts of $B_n{}^\rho$, $B_n{}^\phi$, and $B_n{}^z$ are required. These conditions may also be deduced directly as a consequence of the reflection symmetry at $z = 0, L$.

It is well known that the number of nonzero Hermite coefficients in the representation grows with time [4, 6]. Large errors can result from the truncation of the Hermite series resulting from the absence of Z-array elements above the necessarily finite upper limit on Hermite coefficients M. To control the effect of truncation, we use a 3-D analog of a technique used successfully in 1-D problems [5–7]. A velocity space smoothing term based upon the modified Fokker–Planck operator is introduced on the right-hand side of (1).

$$\delta f/\delta t\,|_c = -\gamma_c(\mathbf{v} \cdot (\partial/\partial \mathbf{v}) + (\partial^2/\partial v^2))f \tag{14}$$

with the corresponding form in the Z representation being

$$\delta Z/\delta t\,|_c = -\gamma_c(s + q + r)\, Z_{sqrnn}(t). \tag{15}$$

Note that the smoothing term depends only on the sum of the Hermite indices so that equivalent relaxation of the Hermite coefficients having the same value of $s + q + r$ is produced by (15).

The form of the smoothing or "collision" term suggests that the triply infinite velocity space Hermite expansions could be terminated along a diagonal in the transform space. Accordingly, only terms in the series for which $q + r + s \leqslant M$ are kept. This has the effect of reducing by a factor of between 4–6, depending on M, the amount of run time and storage required as compared to that for a series with $q, r, s \leqslant M$. This is equivalent to computing all velocity moments up to and including v^M. As a workable choice for γ_c it has been found that $\gamma_c = 1/M$ is satisfactory, i.e., no dramatic numerical instabilities arise and the values for the oscillation frequency and damping decrement in a stable, Maxwellian, homogeneous column tend toward the collisionless, linear analytical values as M increases [5, 6]. The effect of the smoothing term by itself, neglecting all but the time derivative on the left-hand side of (13) would be to produce an exponential relaxation of each Z coefficient from its initial value towards zero. The e-folding time of that relaxation is $M/(s + q + r)$ in dimensionless units. Thus, the larger the value of $s + q + r$, the shorter the relaxation time.

The effects of the smoothing term on the physical properties of the solution can be checked by varying M, the size of the Hermite representation, while holding all other parameters constant and making several runs. As mentioned above, although the results are not collisionless, the convergence towards collisionless values is easily demonstrated in the special, homogeneous case where collisionless,

linear, analytic calculations can be made. Note that the macroscopic charge and currents are represented by coefficients for which $q + r + s = 0$ and 1, corresponding to the "relaxation times" of ∞ and M.

The Field Equations

Equation (13) is in a form which can function as a time derivative operator for each Z element in a time integration algorithm assuming the availability of self-consistent field components. These components must necessarily be calculated from Maxwell's equations (8). This task is greatly simplified by first considering the magnitude of the terms resulting from the operator on the left-hand side of (8), roughly,

$$\left[\nabla^2 - \frac{1}{c^2}\frac{\partial^2}{\partial t^2}\right]\Psi \simeq \begin{cases} \dfrac{1}{l^2\lambda_D{}^2} - \dfrac{\omega^2\omega_p{}^2}{c^2}, & \Psi \text{ (unmagnetized)}, \\ \dfrac{1}{l^2\rho_L{}^2} - \dfrac{\omega^2\omega_c{}^2}{c^2}, & \Psi \text{ (magnetized)}, \end{cases} \tag{16}$$

where l is a characteristic length, ρ_L is the Larmor radius of a thermal particle, and ω_c is the cyclotron frequency. Using these approximations, the ratio for the first term to the second can, in both cases, be shown to be c^2/v_{ph}^2. Thus, providing we are content to look at those processes for which the phase velocity $v_{ph} \ll c$, we may neglect the second, numerically troublesome, term in the operator on the left-hand side of Eq. (8).

Physically, this assumption implies that fields propagate much faster than the fastest particle; and *all* particles experience the effect of a time varying field before *any* particle moves a significant amount. Numerically, this assumption, which is formally equivalent to neglecting the displacement current in Ampere's law, allows the field calculations to be made without regard for plasma source term history. The modified form of (8) used for field calculations, Fourier-transformed and expressed in cylindrical coordinates, is the familiar inhomogeneous Bessel equation

$$\frac{d^2}{d\rho^2}\psi_n + \frac{1}{\rho}\frac{d}{d\rho}\psi_n - \left(\frac{\lambda}{\rho^2} + n^2k^2\right)\psi_n = \chi_n \tag{17}$$

where

$\psi_n(\rho, t)$	λ	$\chi_n(\rho, t)$
$B_n{}^\phi$	1	$-(1/c^2)(nkJ_n{}^\rho - (\partial/\partial\rho)\, J_n{}^z)$
$B_n{}^z$	0	$-(1/c^2\rho)(\partial/\partial\rho)(\rho J_n{}^\phi)$
$E_n{}^\phi$	1	$(1/c^2)(\partial/\partial t)\, J_n{}^\phi$
$E_n{}^z$	0	$nk\tilde{\rho}_n + (1/c^2)(\partial/\partial t)\, J_n{}^z$

(18)

The azimuthal and axial field components for $n > 0$ are calculated as the superposition of a contribution due to plasma source terms within $\rho = b$ and another contribution from the boundary value applied at $\rho = b$. Using the appropriate Dirichlet Green's function, the first contribution becomes an integral over all plasma source terms, and the boundary value contribution is the corresponding homogeneous solution to (17). The field components take the following form.

$$\psi_n(\rho, t) = \int_0^b d\rho'\, \rho' g_\lambda(\rho, \rho')\, \chi_n(\rho', t) + \psi_n(b, t) \frac{I_\lambda(nk\rho)}{I_\lambda(nkb)},$$

$$g_\lambda(\rho, \rho') = I_\lambda(nk\rho_<) \left[\frac{I_\lambda(nk\rho_>)\, K_\lambda(nkb)}{I_\lambda(nkb)} - K_\lambda(nk\rho_>)\right], \tag{19}$$

$$\rho_< = \min(\rho, \rho'), \qquad \rho_> = \max(\rho, \rho').$$

Substitution of (18) into (19) and integrating by parts, we have for $n > 0$,

$$B_n^\phi(\rho, t) = -\frac{nk}{c^2}\left[\left(\frac{I_1}{\alpha_1} - K_1\right)\int_0^\rho d\rho'\, \rho'\{J_n^\rho I_1 + J_n^z I_0\}\right.$$
$$\left. + I_1 \int_\rho^b d\rho'\, \rho' \left\{J_n^\rho \left(\frac{I_1}{\alpha_1} - K_1\right) + J_n^z \left(\frac{I_0}{\alpha_1} + K_0\right)\right]\right\}$$
$$+ B_n^\phi(b, t) \frac{I_1(nk\rho)}{I_1(nkb)}, \tag{20}$$

$$B_n^z(\rho, t) = \frac{nk}{c^2}\left[\left(\frac{I_0}{\alpha_0} - K_0\right)\int_0^\rho d\rho'\, \rho' J_n^\phi I_1 + I_0 \int_\rho^b d\rho'\, \rho' J_n^\phi \left(\frac{I_1}{\alpha_0} + K_1\right)\right]$$
$$+ B_n^z(b, t) \frac{I_0(nk\rho)}{I_0(nkb)}, \tag{21}$$

$$E_n^\phi(\rho, t) = \frac{1}{c^2}\left[\left(\frac{I_1}{\alpha_1} - K_1\right)\int_0^\rho d\rho'\, \rho' I_1 \frac{\partial}{\partial t} J_n^\phi + I_1 \int_\rho^b d\rho'\, \rho' \left(\frac{I_1}{\alpha_1} - K_1\right)\frac{\partial}{\partial t} J_n^\phi\right]$$
$$+ E_n^\phi(b, t) \frac{I_1(nk\rho)}{I_1(nkb)}, \tag{22}$$

$$E_n^z(\rho, t) = nk\left[\left(\frac{I_0}{\alpha_0} - K_0\right)\int_0^\rho d\rho'\, \rho' \left\{\tilde{\rho}_n + \frac{1}{nkc^2}\frac{\partial}{\partial t} J_n^z\right\} I_0\right.$$
$$\left. + I_0 \int_\rho^b d\rho'\, \rho' \left\{\tilde{\rho}_n + \frac{1}{nkc^2}\frac{\partial}{\partial t} J_n^z\right\}\left(\frac{I_0}{\alpha_0} - K_0\right)\right] + E_n^z(b, t) \frac{I_0(nk\rho)}{I_0(nkb)},$$
$$\alpha_\lambda \equiv I_\lambda(nkb)/K_\lambda(nkb). \tag{23}$$

The radial field components for all n are calculated by direct integration of the divergence relations

$$B_n{}^{\rho}(\rho, t) = -\frac{1}{\rho}\int_0^{\rho} d\rho'\, \rho' nk B_n{}^{z}(\rho, t), \tag{24}$$

$$E_n{}^{\rho}(\rho, t) = \frac{1}{\rho}\int_0^{\rho} d\rho'\, \rho'(\tilde{\rho}_n(\rho, t) + nkE_n{}^{z}(\rho, t)). \tag{25}$$

These calculations are carried out with axial fields on the right-hand sides which are newly computed from (21) and (23). In this manner, all field components are calculated from and consistent with the instantaneous sources (plasma charge and current densities as well as external fields affecting the plasma through the boundary values at $\rho = b$).

For $n = 0$, we find the perfect reflection condition on each end of the periodicity length L requires that there be no $J^z_{n=0}$ and therefore no $B^{\phi}_{n=0}$. Similar arguments can be used on the charge density to show that $E^z_{n=0}$ is necessarily zero. Thus only the $E^{\phi}_{n=0}$ and $B^z_{n=0}$ components need to be calculated; this is accomplished by direct integration of (17).

$$E^{\phi}_{n=0}(\rho, t) = \frac{\rho}{b}\left[\frac{1}{c^2 b}\left\{\frac{(b^2 - \rho^2)}{\rho^2}\int_0^{\rho} d\rho'\, \rho' \int_0^{\rho'} d\rho''\, \frac{\partial}{\partial t} J^{\phi}_{n=0}\right.\right.$$

$$\left.\left. - \int_{\rho}^{b} d\rho'\, \rho' \int_0^{\rho'} d\rho''\, \frac{\partial}{\partial t} J^{\phi}_{n=0}\right\} + E^{\phi}_{n=0}(b, t)\right], \tag{26}$$

$$B^z_{n=0}(\rho, t) = \frac{1}{c^2}\int_{\rho}^{b} d\rho'\, J^{\phi}_{n=0} + B^z_{n=0}(b, t). \tag{27}$$

Despite the complicated appearance of the integrals for the field components (20)–(27) their evaluation at each time step is simplified because only the sources vary in time. All of the functions except the sources are evaluated only once per run and are then stored for use in the calculation of the fields at each time step. The field calculations require negligible computer time compared to the dynamical equation. Also, a variety of boundary conditions can be used with no modifications other than changing input parameters.

II. Self-Consistent Time Integration

Equations (13) and (20)–(27) constitute a set of equations that can be written as a computer algorithm to follow the nonlinear evolution in time of the palsma column. The flow chart given in Fig. 2 shows the procedure used to integrate both

the Z array and the self-consistent fields by means of a second-order Runge–Kutta algorithm. The essential feature which allows the nonlinear solution to be followed in time is that new field components are calculated from the most recent Z array before calculation of the new time-advanced Z array.

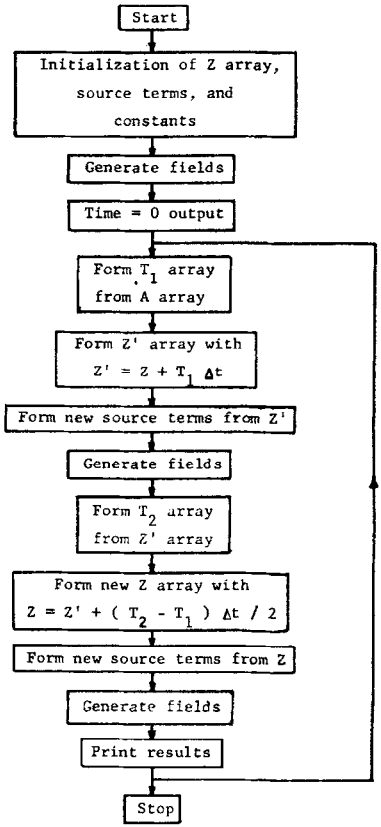

FIG. 2. The time integration flow chart

III. NUMERICAL PROCEDURE

Since the general method of initializing the distribution function is to add small perturbations to inhomogeneous equilibria, one necessarily knows the zeroth-order radial profiles of the charge and current density at $t = 0$. We have found that by scaling out the charge density profile in each Z element, much less accuracy

(implying less computation time) is required of the finite difference approximation necessary to evaluate (13). If we make the replacement

$$\begin{aligned} Z(\rho_\eta\,,\,t) &= g_\eta(\rho_\eta)\,Z^*(\rho_\eta\,,\,t), \\ g_\eta(\rho_\eta) &\equiv Z_{s=q=r=0,\eta,n}(\rho_\eta\,,\,t=0), \end{aligned} \tag{28}$$

then the finite difference becomes

$$\frac{\Delta Z_{\eta,n}(\rho_\eta\,,\,t)}{\Delta\rho} = g_\eta(\rho_\eta)\left[\frac{Z^*_{\eta,n}}{g_\eta(\rho_\eta)}\frac{dg_\eta(\rho_\eta)}{d\rho} + \frac{(Z^*_{\eta+1,n} - Z^*_{\eta-1,n})}{\Delta\rho}\right]. \tag{29}$$

After substitution of (28) and (29) into (13), $g_\eta(\rho_\eta)$ is divided out of (13). The finite differences near the grid endpoints are approximated by Taylor series.

The advantage of this scheme is that the basic equilibrium profile is easier to maintain with small numbers of grid points at large spacing. While other Z coefficients may not have the same profile as that of the charge density, they are not rendered more difficult to compute. We find that for most subscript sets (s, q, r, η, n) that the accurately known first term on the left-hand side of (29) dominates the expression.

In stable cases where the z-independent radial profile does not change rapidly away from its initial value, a further saving of computation time can be realized by neglecting all the zeroth-order contributions to the $n = 0$ time derivatives. Since the zeroth-order terms cancel exactly for the equilibrium, initially and for a short time, the dominant contributions to the $n = 0$ time derivatives is from second-order terms contained in the convolution sum. In runs where the results are the same whether or not the zeroth-order terms are included, computer time can be saved in parameter studies by neglecting these terms.

The field integrations are also initialized using the known radial dependence of the initial source terms. The basic integration algorithm is based on a Taylor's series expansion of the integrand about a point midway between two grid points. Expanding through third order and integrating term by term, we have

$$\begin{aligned} &\int_{\rho_\eta}^{\rho_{\eta+1}} f(\rho')\,d\rho' \simeq \Delta\rho\, f(\rho)\Big|_{\rho_i} + \frac{\Delta\rho^3}{24} f'(\rho)\Big|_{\rho_i}, \\ &\rho_i = (\rho_\eta + \rho_{\eta+1})/2, \qquad \Delta\rho = \rho_{\eta+1} - \rho_\eta \end{aligned} \tag{30}$$

with the even powers of $\Delta\rho$ dropping out. Looking at the integrands in (20)–(27), all can be written as the product of a source term $S_n(\rho, t)$ and the time-independent Green's function of radius $R_n(\rho)$ in terms of modified Bessel functions. Thus the right-hand side of (30) becomes

$$\begin{aligned} &\Delta\rho\, R_n(\rho_\eta)\, S_n(\rho_\eta\,,\,t) \\ &\quad + (\Delta\rho^3/24)[R_n''(\rho_\eta)\, S_n(\rho_\eta\,,\,t) + 2R_n'(\rho_\eta)\, S_n'(\rho_\eta\,,\,t) + R_n(\rho_\eta)\, S_n''(\rho_\eta\,,\,t)]. \end{aligned} \tag{31}$$

The radial function $R_n(\rho)$ and its derivatives are evaluated initially by polynomial approximation and may be determined very accurately, providing the liberty of using very simple interpolation and difference techniques to determine the source functions and derivatives between grid points.

It has proven expedient to "teach" the algorithm to calculate very accurately the equilibrium fields given the equilibrium charge and current densities. The necessary modifications, determined by ratios between calculated and known equilibrium fields, are incorporated directly into the appropriate set of functions $R_n(\rho)$ during the initial evaluation. For the usual applications, these correction correction factors have not deviated from unity by more than 5%.

IV. The Unstable Electrostatic Column

Initial studies have been made on both stable Maxwellian and two-stream unstable electrostatically contained columns in which the magnetic field has been eliminated by assuming the velocity of light to be infinite. The stable results have been presented elsewhere [2, 3]. The Gaussian electron profile in radius is contained by a radial electric field which results from an excess positive charge within the column.

The unstable equilibrium profile is

$$f = (2\pi)^{-3/2} \exp(-\rho^2/d^2)\, v_z^2 \exp(-v^2/2) \tag{32}$$

for the electrons and, for the ions,

$$f_{\text{ion}} = (2\pi)^{-3/2}[\exp(-\rho^2/d^2) + 4/d^2] \exp(-v^2/2). \tag{33}$$

The containing field may be shown to be

$$E^{\rho}_{n=0}(\rho) = 2\rho/d^2. \tag{34}$$

Running with four grid points (starting at $\rho = 3\lambda_D$ and spaced every $6\lambda_D$), two Fourier modes, and between 13–17 Hermite coefficients in each velocity coordinate, small sinusoidal axial current perturbations of the form $j_z = (2\pi)^{-3/2}\epsilon \exp(-\rho^2/d^2) \cos(kz)$ are added to (32) to initially perturb the equilibrium. The exponential growth which characterizes the two-stream instability is evident in both $n = 1$ field components near the axis at $\rho = 3\lambda_D$ (Figs. 3 and 4). The growth rates in both components are greatly diminished for all k/k_D by increasing the inhomogeneity (Fig. 5). The $n = 2$ components at $\rho = 3$ grow at approximately twice the corresponding $n = 1$ growth rates, as predicted by linear theory.

Attempts to demonstrate clearly the nonlinear limitation of exponential growth

have been unsuccessful, due, at least in part, to the reduced growth rate resulting from the inhomogeneity. A similar run in the homogeneous limit ($d = \infty$) indicates a relatively abrupt nonlinear limitation of $E^z_{n=1}$ at approximately $t = 33\omega_p^{-1}$. It is apparent in Figs. 3 and 4 that the exponential growth rate of the field components decrease with time. This nonlinear effect suggests that a limit exists and that the limitation will not be as abrupt as in the homogeneous case.

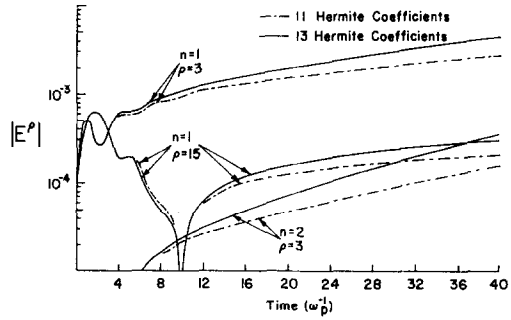

FIG. 3. E_n^ρ unstable time profile with $M = 13$, NG $= 4$, $\Delta\rho = 6$, $d = 10$, $N = 3$, $\epsilon = 0.02$ and $\Delta t = 0.1$.

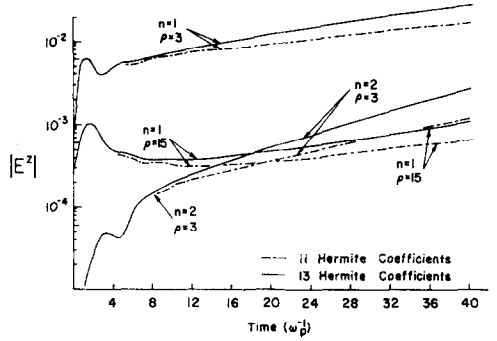

FIG. 4. E_n^z unstable time profile corresponding to E_n^ρ profile in Fig. 3.

The $n = 1$ radial electric field at $\rho = 15$ (Fig. 3) exhibits a nonphysical change in sign at $t \sim 10\omega_p^{-1}$. It has been determined that this sign change is produced by a mild grid instability which, for the parameter sets of interest here, has always contained less than 1 % of the total field energy of the system. Similar runs with the grid spacing $\Delta\rho$ reduced by a factor 2 and with twice the grid points more than triples the time at which the difficulty appears.

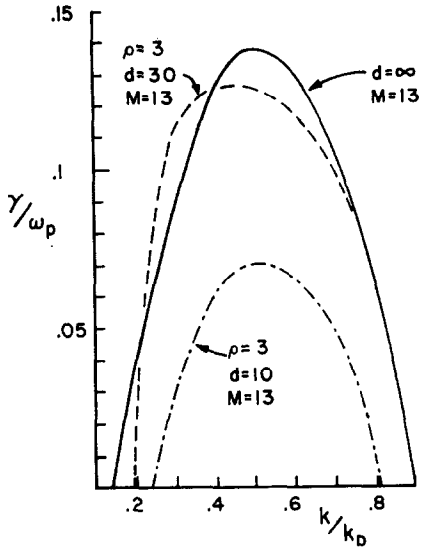

FIG. 5. Axial unstable γ/ω_p vs k/k_D at $\rho = 3$ from runs using $M = 13$, NG $= 4$, $\Delta\rho = 6$ and $\Delta t = 0.1$ for $d = 10, 30, \infty$.

V. ACCURACY OF THE SOLUTION

The usual means of ascertaining the convergence of the several expansion methods utilized is to increase the number of terms or grid points of the representation in question. One of the more obvious convergence questions concerns the accuracy of the finite differenced radial derivatives. As a standard of comparison, a run with parameters of $s\,\Delta\rho$ (the radial position of the first grid point) $= 3$, NG (the number of grid points) $= 8$, $\Delta\rho$ (the grid spacing constant) $= 6$, $d = 30$, 13 Hermite coefficients, 3 Fourier modes, and $\Delta t = .1$ was made. Doubling $\Delta\rho$ to $6\lambda_D$ in a similar run to test grid convergence caused a variation in $E^z_{n=1}$ ($\rho = 15$) of approximately .4% after $9\omega_p^{-1}$. The radial electric field is more strongly dependent upon the grid size, as one would expect by comparing (23) and (25). In the $E_n{}^z$ calculation, the Green's function integration tends to smooth the coarse radial representation of the charge density. The absence of this smoothing in the $E_n{}^\rho$ calculation is evident in the greater .7% deviation between the radial electric fields at $\rho = 15$ and $9\omega_p^{-1}$ in these same two runs.

As previously mentioned, the parameter set $\Delta\rho = 6$, $d = 10$ is mildly susceptable to grid instability on the outer grid points. The instability does not appear in the stable Landau damping runs [2, 3] using these grid parameters. Decreasing the inhomogeneity ($d = 30$), doubling NG while reducing $\Delta\rho$ by a factor of 2 permits

unstable runs to be made in excess of $t = 25\omega_p^{-1}$ without difficulty. The nonphysical sign change does reappear in $E^{\rho}_{n=1}$ ($\rho = 21$) at $t \sim 14\omega_p^{-1}$ for $d = 30$ if $\Delta\rho$ is increased to 6 and NG dropped to 4. The conclusion is that for initializations that will deviate rapidly and significantly from the initial radial profile, either several more grid points are necessary or the scaling procedure (28) will have to be reevaluated on a periodic basis.

The order of the Hermite representation M has a significant effect on the growth and decay rates of the plasma. Since the collision frequency of the collision term (15) is the inverse of M, collisional damping increases as M decreases. The additional damping resulting from finite M is clearly apparent in comparing the homogeneous ($d = \infty$), growth rates for various values of M (Fig. 6). A similar but less extensive investigation of the finite d cases for $M = 10$ and 12 indicates generally that runs with finite d have the same dependence on M as the homogeneous results.

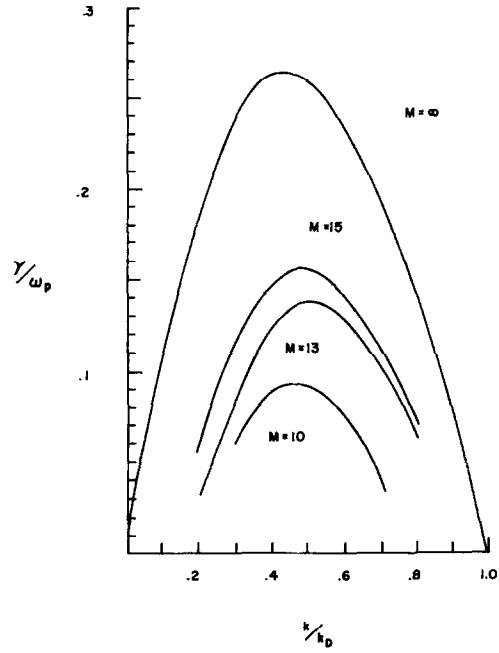

FIG. 6. Axial unstable γ/ω_p vs k/k_D for various M in the homogeneous ($d = \infty$) limit.

Almost all runs have been made with the 0, 1 and 2 Fourier modes, and as predicted by linear theory, the $n = 2$ modes grow exponentially at twice the $n = 1$ growth rate [3, 4]. It is apparent that several additional Fourier modes are necessary

for runs extended in time in excess of $40\omega_p^{-1}$. As shown in Figs. 3 and 4, for short time periods initialized with small $n = 1$ current perturbations, the amplitude of the $n = 2$ field components are at least a factor of 10 smaller than the $n = 1$ components, containing only a negligible 1 % of the total field energy. Thus, for growth rate studies obtained from runs approximately $12\text{–}15\omega_p^{-1}$ in time, retaining only the first 3 Fourier modes produced adequate accuracy.

Convergence of the time integration has been investigated by running identical parameter sets with the exception of the time step. For example, reducing Δt by a factor of 2 in the run used for comparison above, we have demonstrated that the two electric field components do not change by more than .5 % after being integrated in time $9\omega_p^{-1}$. The agreement near the axis (that is, ρ_1) is better than .1 % for the same period.

VI. Comparison with Other Relevant Work

Most previous studies in two-dimensional cylindrical geometry have been carried out in the limit of infinitely strong axial magnetic fields, effectively limiting the dynamics to one dimension. Most notably, qualitative agreement has been found with the analytic work of Lee [8], Book [9], and Harris [10] when radial motion is eliminated in the simulation code. The conclusion by Harris that for

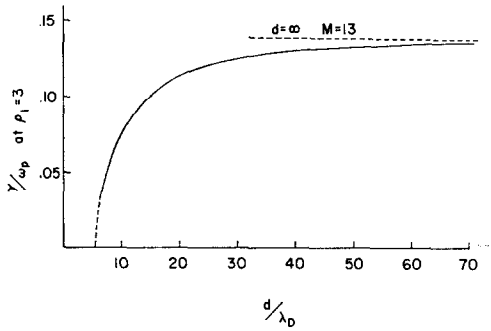

FIG. 7. Axial unstable γ/ω_p vs d/λ_D for $E^z_{n=1}(\rho = 3)$ at $k/k_D = 0.5$ with $M = 13$.

sufficiently strong inhomogeneity even the most unstable wavenumber can be stabilized appears to be supported even including radial currents (Fig. 7). The results of both Lee and Book were obtained in the limit of small k/k_D and, as such, were useful primarily in that qualitative effects of the inhomogeneity could be established for $k/k_D \leqslant .3$.

VII. Summary

The techniques presented here have a far greater range of applicability than the unstable results presented here indicate. Both the stable [2] and unstable results are consequences of applying these techniques to the "standard test" that plasma simulations codes must handle. Of primary importance thus far has been the establishment of the early tendencies of the stable [2] and unstable plasma column which have realistic radial inhomogeneity.

One of the most interesting capabilities is the ease with which one can recover nonlinear effects in the velocity profile by resumming the Hermite series [2]. Such detail in more than one dimension has been difficult if not impossible to demonstrate by other simulation techniques.

Acknowledgments

The author wishes to thank Dr. Thomas P. Armstrong for suggesting the approach used in this work. Additional thanks are due to J. P. Friedberg and H. Weitzner for useful discussions.

This work was supported in part by a General Research Grant at the University of Kansas and by additional computing support at the University of Kansas. Additional computer support has been provided through the courtesy of the Los Alamos Scientific Laboratory, Los Alamos, NM, and the Johns Hopkins Applied Physics Laboratory, Silver Spring, MD.

References

1. R. L. Morse and C. W. Nielson, One-, two-, and three-dimensional numerical simulation of two-beam plasmas, *Phys. Rev. Lett.*, **23** (1969), 1087–1090; C. K. Birdsall and D. Fass, Clouds-in-clouds, clouds-in-cells, physics for many-body plasma simulation, *J. Computational Phys.* **3** (1969), 494; G. Joyce and G. Knorr, Nonlinear evolution of the dory–guest–harris instability, *Phys. Fluids* **15** (1972), 177–182.
2. D. W. Hewett and T. P. Armstrong, *Phys. Fluids* (1973) to be published.
3. D. W. Hewett, Ph.D. Thesis, University of Kansas, Department of Physics and Astronomy, May 1973.
4. T. P. Armstrong, Numerical studies of the nonlinear Vlasov equation, *Phys. Fluids* **10** (1967), 1269–1280.
5. T. P. Armstrong, R. C. Harding, G. Knorr and D. Montgomery, Solutions of Vlasov's equation by transform methods, *in* "Methods of Computational Physics," Vol. 9 Academic Press, New York, 1970.
6. F. C. Grant and M. R. Feix, Fourier–Hermite solutions of the Vlasov equations in the linearized limit, *Phys. Fluids* **10** (1967a), 696–702.
7. F. C. Grant and M. R. Feix, Transition between Landau and van Kampen treatments of the Vlasov equation, *Phys. Fluids* **10** (1967b), 1356–1357.
8. K. F. Lee, Streaming instabilities with zero-order density gradients, *Phys. Fluids* **9** (1966), 2435.

9. D. L. BOOK, Landau damping and growth of electrostatic modes with effects of spatial variation, *Phys. Fluids* **10** (1967), 198.
10. E. G. HARRIS, Two-stream instabilities in a cold inhomogeneous plasma in a strong magnetic field, *Phys. Fluids* **7** (1964), 1572–1577.